
Article:
Kozak, L., Kronberg, E.A., Petrenko, B. et al. (4 more authors) (2023) Turbulent dipolarization regions in the Earth's magnetotail: ion fluxes and magnetic field changes. Frontiers in Astronomy and Space Sciences, 10.

https://doi.org/10.3389/fspas.2023.1226200

---

frontiers | Frontiers in Astronomy and Space Sciences

TYPE Original Research
PUBLISHED 13 October 2023
DOI 10.3389/fspas.2023.1226200

OPEN ACCESS

EDITED BY
Joseph E. Borovsky,
Space Science Institute (SSI), United States

REVIEWED BY
Victor Sergeev,
Saint Petersburg State University, Russia
Marina Stepanova,
University of Santiago, Chile

*CORRESPONDENCE
Liudmyla Kozak,
gutovska@ukr.net

RECEIVED 20 May 2023
ACCEPTED 26 September 2023
PUBLISHED 13 October 2023

CITATION
Kozak L, Kronberg EA, Petrenko B, Blöcker A, Akhmetshyn R, Ballai I and Fedun V (2023), Turbulent dipolarization regions in the Earth's magnetotail: ion fluxes and magnetic field changes. *Front. Astron. Space Sci.* 10:1226200. doi: 10.3389/fspas.2023.1226200

Turbulent dipolarization regions in the Earth's magnetotail: ion fluxes and magnetic field changes

Liudmyla Kozak[1,2]*, Elena A. Kronberg[3], Bohdan Petrenko[1,2], Aljona Blöcker[3], Roman Akhmetshyn[1], Istvan Ballai[4] and Viktor Fedun[5]

[1]Department Astronomy and Space Physics, Taras Shevchenko National University of Kyiv, Kyiv, Ukraine, [2]Space Research Institute of the National Academy of Sciences of Ukraine, The State Space Academy of Ukraine, Kyiv, Ukraine, [3]Geophysics, Department of Earth and Environmental Sciences, University of Munich, Munich, Germany, [4]Plasma Dynamics Group, School of Mathematics and Statistics, The University of Sheffield, Sheffield, United Kingdom, [5]Plasma Dynamics Group, Department of Automatic Control and Systems Engineering, The University of Sheffield, Sheffield, United Kingdom

In this work, we consider the dynamics of ion fluxes and magnetic field changes in turbulent regions of magnetotail dipolarizations. The data from the Cluster-II mission (magnetic field measurements from fluxgate magnetometers and energetic charged particle observations from RAPID spectrometers) were used for the analysis. We study individual events and investigate statistically the changes of charged particle fluxes during magnetic field dipolarizations observed during 2001–2015. Received changes in the spectral index indicate that CNO+ ions undergo stronger acceleration during dipolarization than protons and helium ions. Before dipolarization front monotonic growth the ions flux is observed (the maximum of flux is observed at 1–1,5 min after the start of dipolarization) in the range of ~ 92–374 keV for proton; in the energy range ~ 138–235 keV for He+ and in the energy range of 414–638 keV for CNO+ ions. Flux increase before arriving dipolarization front may result from the reflection of plasma sheet ions at the dipolarization front and the result of the resonant interactions of ions with low-frequency electromagnetic waves.

KEYWORDS

dipolarization fronts, charged particles, differential fluxes, waves, superimposed epoch analysis

1 Introduction

One way to obtain information about the state of astrophysical plasma is by studying the radiation they emit and that we remotely observe. Therefore, it is of essential importance to understand the mechanisms that contribute to the generation of radiation. Due to large-scale shear movements, shock waves, jets, etc., astrophysical plasma (Hajivassiliou, 1992; Arzoumanian et al., 2011; Brandenburg and Nordlund, 2011;) and near-Earth plasma (Saur, 2004; Uritsky et al., 2011; Alexandrova et al., 2013; Bruno and Carbone, 2013; Von Papen et al., 2014) enter a turbulent state. At the same time, remote observations of turbulence and the evolution of plasma energy in astrophysical plasma can provide only integrated results, and are mostly considered only within the framework of one or another model. In this regard, the near-Earth environment is a preferred laboratory for analysing

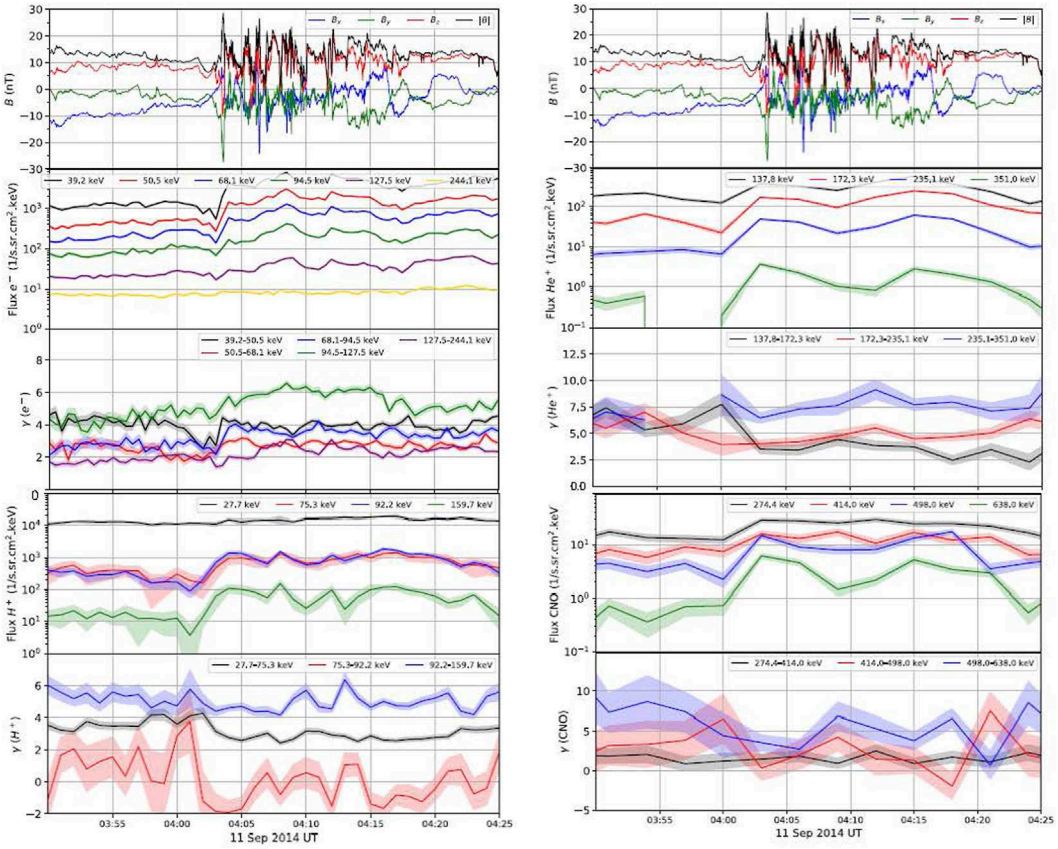

FIGURE 1
Changes in the magnetic field, fluxes and spectral index for the event of 11 September 2014. The intensities are averaged over a sampling interval of 30s for e−, 60s for H+, and 180s for CNO+ and He+. Spectral indices γ are calculated from the ion intensities using Eq. 1. The bands in the ion and electron fluxes show the standard deviations obtained from the instrument and the bands in the spectral index represent the uncertainty in γ using error propagation of the errors in the ion and electron intensities.

turbulent processes, since we can use *in situ* observations to obtain information about the dynamical state of the plasma and the variation of the characteristic plasma parameters. In turbulent regions, energy enters the system on large scales, and then it is transferred to smaller scales through nonlinear interactions (turbulent energy cascade). Since energy dissipation becomes significant on small scales, where the scale of turbulent fluctuations becomes comparable to the particle gyroradius, the nature of turbulent processes and the scale of their changes depend significantly on the content of heavy ions (Kozak et al., 2018). In turn, the dissipation of turbulent fluctuations leads to plasma heating and acceleration of charged particles.

The question of how heating occurs due to turbulent motions remains open. Another important question is whether the heating will be associated only with localized structures, or is distributed more evenly throughout the volume. Both possibilities are related to the redistribution of particles by energies through a sequence of both linear and non-linear processes (Servidio et al., 2009; Chandran et al., 2010; Camporeale and Burgess, 2011; Servidio et al., 2012; Karimabadi et al., 2013; TenBarge and Howes, 2013). At the same time, localized dissipation is associated with the phenomenon of "intermittency", which is an uneven distribution of energy within a turbulent environment.

Observations of solar wind plasma show that heavier ions (in particular, alpha particles) provide a much more efficient heating than protons (Kasper et al., 2008). Dissipation of kinetic Alfvén waves (KAW) by stochastic heating is also more efficient for heavier ions, indicating a privileged channel for alpha particle heating and energy dissipation in the solar wind (Chandran et al., 2013). Turbulent heating and acceleration of alpha particles due to the dissipation of cyclotron waves are considered in the study by (Maneva et al., 2013). Such waves can be effective for feeding heavier ions and for generating complex velocity distribution functions and temperature anisotropy (Telloni et al., 2007; Grigorenko et al., 2015; Malykhin et al., 2018; Malykhin et al., 2019). Wave damping also plays an important role in heating and accelerating heavier ions in shock wave regions (Kronberg et al., 2009).

Both the solar wind and ionosphere can serve as sources for ions and electrons in the magnetosphere (Delzanno et al., 2021). The source of ions can be determined based on the property that ionospheric particles are singly ionized, while solar wind ions are almost completely ionized. The number of ions entering the

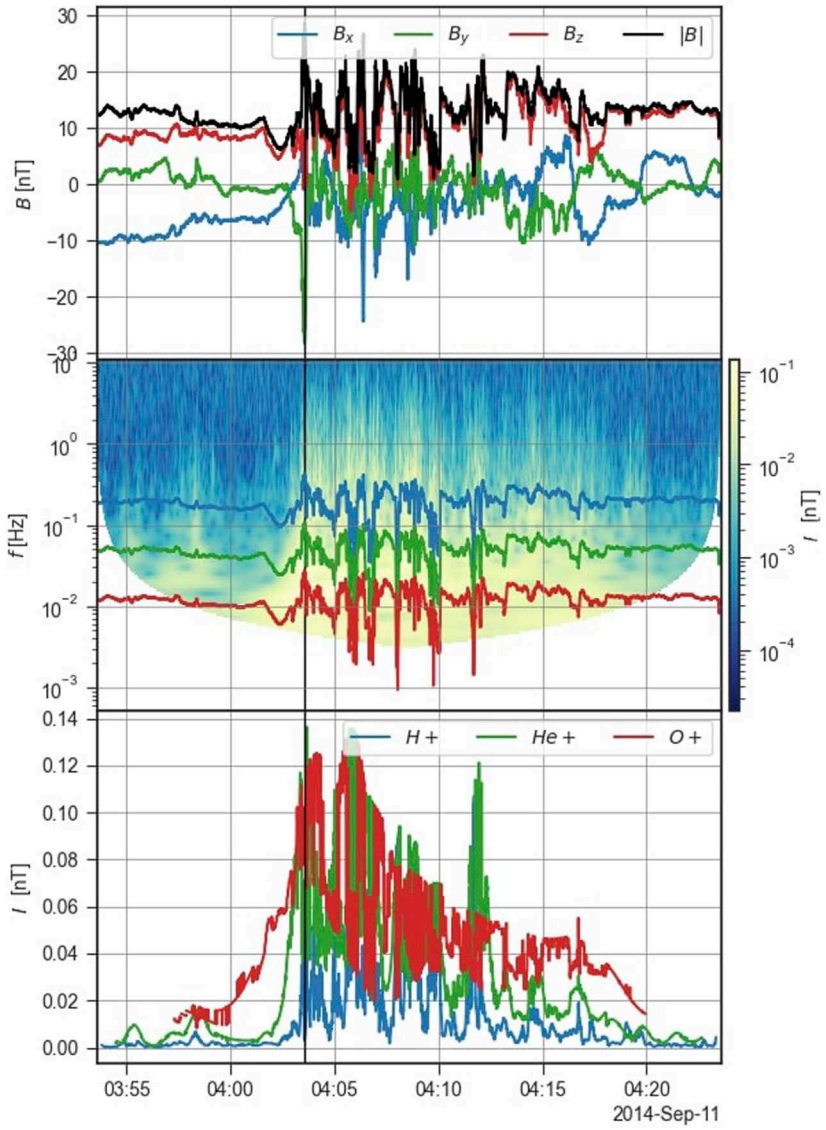

FIGURE 2
The value of the intensity of magnetic field oscillations at different gyrofrequencies for the event of 11 September 2014, as measured by C4. The top panel shows magnetic field changes for 11 September 2014 event. The middle panel indicates the square root of the wavelet power of the magnetic field vector with overplotted gyrofrequencies of H+, He+, and O+. The bottom panel shows wavelet amplitudes along each gyrofrequency in the time domain.

magnetosphere will depend on the level of geomagnetic activity. It can be determined by a significant number of factors, including solar wind ion heating at the front of the shock wave, the modulation in the region of magnetic field reconnection, etc.

The presence of heavy ions in the magnetosphere will significantly change the physics of the processes taking place there. Since the main characteristics of the plasma (density, temperature, pressure, Alfvén velocity, thickness of the current/plasma layer) are changing, the conditions and rate of development of instabilities (in particular the Kelvin-Helmholtz instability and reconnection) will also change.

According to our current understanding, the main factors affecting the dynamics of electron and ion fluxes in the Earth's magnetosphere include the EUV radiation from the Sun, reconnection events in the magnetopause region, particle acceleration, etc. (Kronberg et al., 2014). As a result of such dynamical events, charge particles may be subject to prominent energization up to the hundreds of keV range (e.g., (Ipavich et al., 1984; Keika et al., 2011)). Repeated enhancements of the energetic O+ content in conjunction with repeated auroral intensifications were observed by Mitchell et al. (2003). Evidence of a mass-dependent energization in the ~ 10–210 keV/e range during substorms in the near-Earth plasma sheet was also presented by Möbius et al. (1987) and Kistler et al. (1990), Retinò et al. (2007), Chasapis et al. (2015), Malykhin et al. (2018), Malykhin et al. (2019).

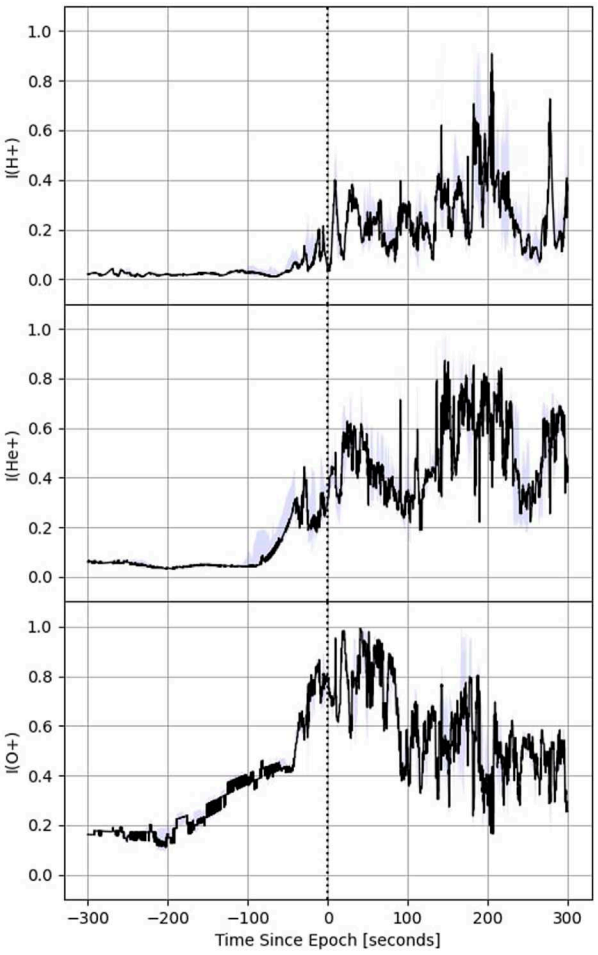

FIGURE 3
Change in the intensity of wavelet oscillations at gyrofrequencies of various types of ions from four-spacecraft measurements for 11 September 2014 event. Zero value for Time Since Epoch indicates the first dipolarization front. Superposed epoch analysis was performed for all Cluster spacecraft for this event. Blue shadows mean an area between the 25th and 75th percentiles. The black line is the median value.

The energy of charged particles in the Earth's magnetosphere changes significantly with a sudden change in the reconfiguration of the magnetic field from a stretched to more dipole configuration (dipolarization). Observations from space vehicles showed that the rapid changes of B_z component of the magnetic field represent the spatial structures, i.e., the fronts of dipolarization (DF) moving towards the Earth (Nakamura et al., 2002; Runov et al., 2011). The DFs are often associated with bursty bulk flows (BBFs) (Angelopoulos et al., 1992). These flows can be responsible for energy and mass transfer from far regions of the magnetospheric tail to distances of about 10 Earth's radii, where the flows are decelerated (Shiokawa et al., 1997). The dipolarization fronts can be detached as (i) isolated (observed over a few minutes) (Nakamura et al., 2002; Runov et al., 2009; Runov et al., 2011) and (ii) "secondary" (with duration up to hours), which are associated with the system of currents (wedge) during substorm generation (Sergeev et al., 2012). The properties and behaviour of various ion fluxes during magnetic field dipolarization, which are characterized by turbulence and significant variability of plasma parameters, were considered in the studies by Kozak et al. (2018b), Kozak et al. (2018a), Kozak et al. (2018), Kozak et al. (2020), Kozak et al. (2021).

The results presented in the studies by Kozak et al. (2018) showed that the relative content of heavy ions in the observed regions of magnetic field dipolarization may exert significant influence upon the scale of the transition from the magnetohydrodynamic to the kinetic approach in the analysis of turbulent processes.

The aim of this study is to use measurements of the magnetic field and particle fluxes in various energy channels to estimate the time dependence of these values before and after the start of dipolarization; to find out the energization evolution of protons and heavier ions.

In the first part of our study, we investigate the change in fluxes of charged particles and magnetic field changes for a single event. Later we will provide a statistical analysis of the change in particle fluxes in the region of magnetic field dipolarization observed during 2001–2015 using the superimposed epoch approach.

2 Observational data

For our analysis, we used the magnetic field measurements provided by fluxgate magnetometers (FGM) on board four Clusters spacecraft (SC) with resolution 22.4 Hz (Balogh et al., 2001), and fluxes measurements by RAPID (Research with Adaptive Particle Imaging Detectors) spectrometers in the energy range up to 1,500 keV for protons with the resolution 0.25 Hz, and up to 4,000 keV for heavier ions with 0.067 Hz (Wilken et al., 2001).

Unless otherwise noted, we used GSM (geocentric solar magnetospheric) coordinate system everywhere.

Localization of the source of injection can be established by the signal delay between spacecraft. Accordingly, if the flow reinforcement is observed simultaneously in an extensive energy range means that the space vehicle is close to the injection source (non-dispersion injection), while if the satellite is far from the source the delay in the flow change is observed, that is first the more energetic particles come in, then low-energetic ones (also called dispersion injection) (for example (Zaharia et al., 2000; Kronberg et al., 2017; Malykhin et al., 2018;)).

All analysed events are characterized by multiple dipolarization and correspond to criteria (Borovsky et al., 1993):

- sharp fluctuations B_z components of the magnetic field (≥4 nT);
- large inclination angle of magnetic field (≥45°);
- large inclination angle from minimal to maximal B_z (≥10°);
- value $|B_x| \leq 15$ nT.

The beginning of the first dipolarization front for the considered events is shown in Supplementary Appendix Table S1. Initialization of the substorm and dipolarization of the magnetic field for all events takes place in a spatial range $-10 > X_{GSE} > -17R_E$, $-5 < Y_{GSE} < 9R_E$ and $-1 < Z_{GSE} < 4R_E$. As a typical example of ion flux changes in magnetotail regions, we consider in detail the event on 11 September 2014.

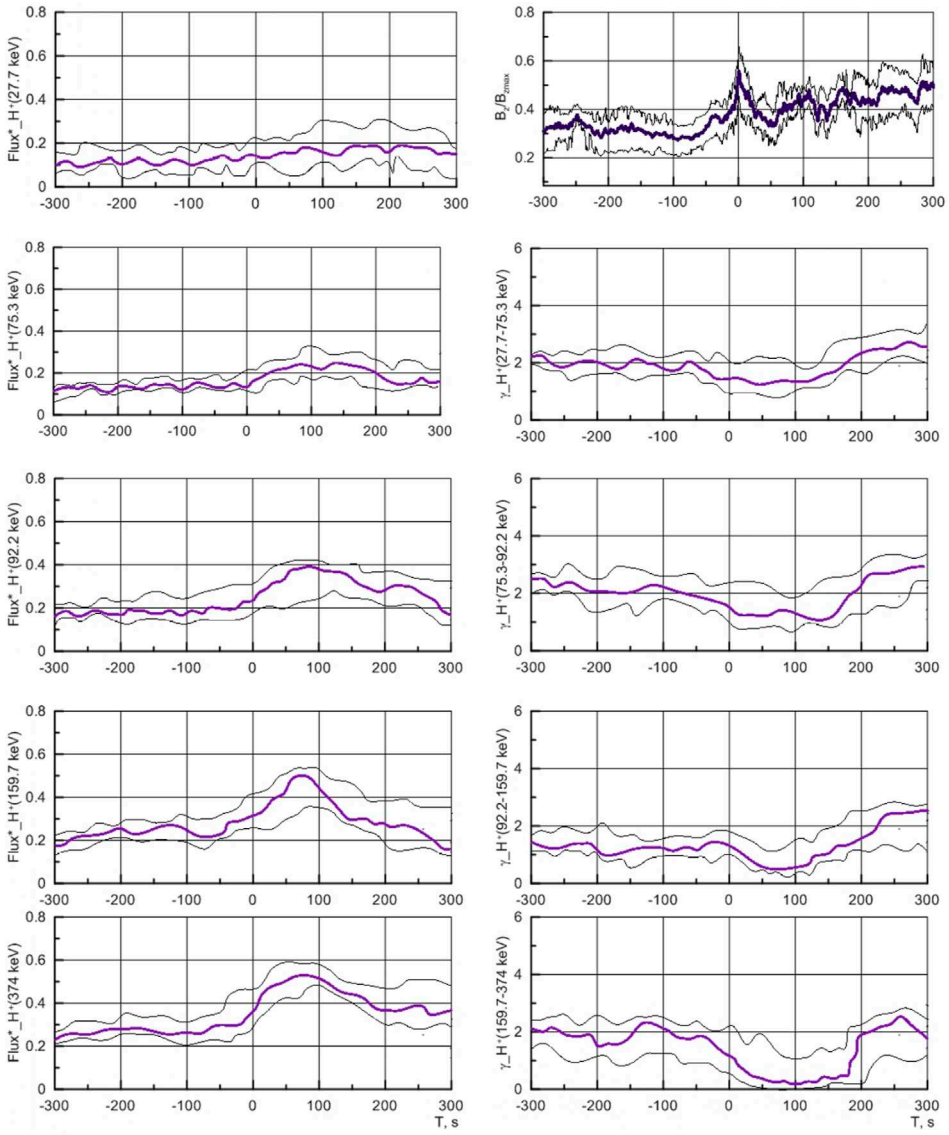

FIGURE 4
Normalized proton fluxes (left) and spectral index (right) in different energy channels relative to the beginning of dipolarization by the superposed epoch method. The top right panels correspond to magnetic field changes (also applied to the superimposed epoch method). Black lines show the scatter of values.

3 Results

3.1 Event study

For the 11 September 2014 event, the dipolarization (a sharp increase in the B_z component of the magnetic field pointing north) in the magnetotail begins at around 04:03:13 UT. The onset of dipolarization becomes evident through a pronounced jump in the B_z component. Figure 1 shows the temporal evolution of the magnetic field (top panel).

For this event, a series of injections at SC are presented in Supplementary Appendix Table S2. We determined proton injections as increases in proton flux in, at least, two energy channels by more than 5 times, and electron injections as increased more than 1.7 times (Malykhin et al., 2018). In the case of protons, we record a smaller number of injections, and there is a shift between proton and electron injections.

The difference in observations of electron and proton injections can also be attributed to the complex structure of the flux accumulation region, consisting of several pulses moving one after the other. The presence of several localized pulses complicates the multiscale picture of magnetic field gradients, which affects the electron drift trajectories and cause the formation of multiple and short electron injections rather than a monotonous increase of suprathermal electron flux.

Further, we compare changes in electron and ion fluxes with magnetic field changes (top panel of Figure 1). The energy

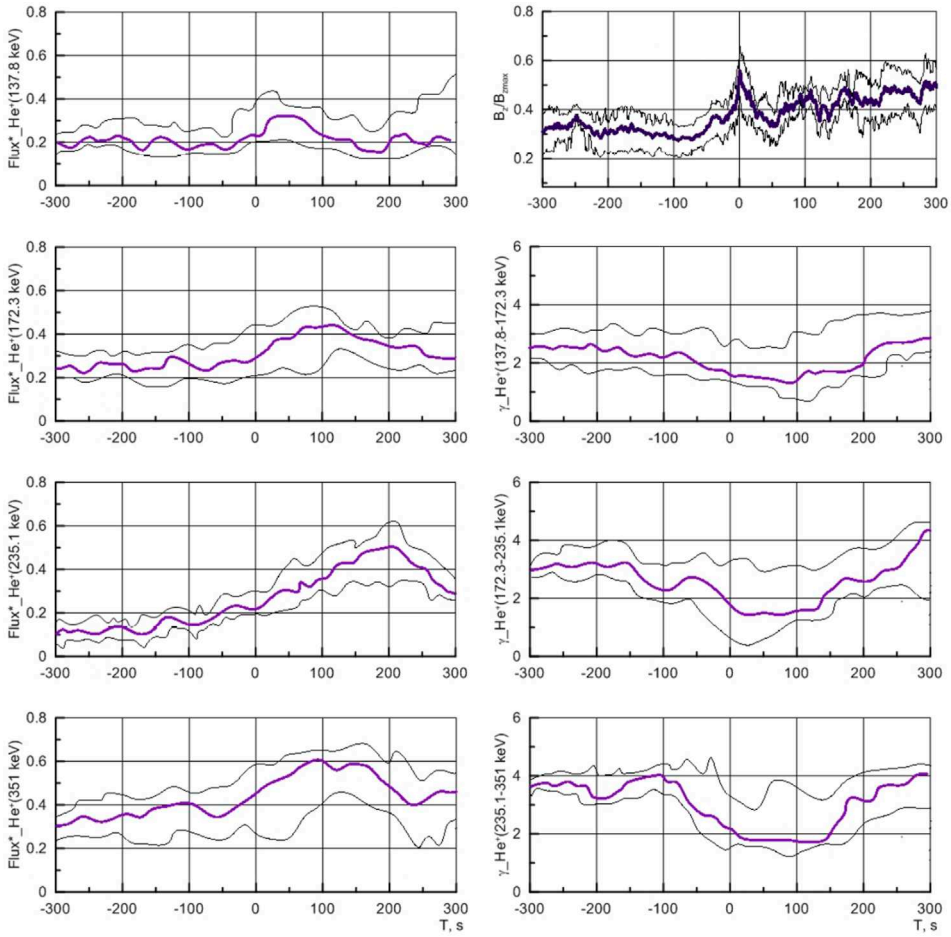

FIGURE 5
Normalized proton fluxes (left) and spectral index (right) in different energy channels relative to the beginning of dipolarization (zero point) by the superposed epoch method. The top right panels correspond to magnetic field changes (also applied to the superimposed epoch method). Black lines show the scatter of values.

dependency of fluxes was considered in the form of a power law: Flux ~ Energy$^{-\gamma}$ (Imada et al., 2007).

The ratio to determine the spectral index was determined as (Kronberg and Daly, 2013):

$$\gamma = -\frac{\ln\left(\frac{J_{i2}}{J_{i1}}\right)}{\ln\left(\frac{E_{eff2}}{E_{eff1}}\right)}, \quad (1)$$

where J_{i2} and J_{i1} - are the differential fluxes of charged particles in neighbouring energy channels. As effective energies, E_{eff2} and E_{eff1} we use the geometric mean between the lowest energies of the neighboring channels.

The fluxes measured by the RAPID experiment and the calculated values of the spectrum index for the event of 11 September 2014, are presented in Figure 1. Averaging was carried out in the time resolution of 30 s for electrons, 60 s for H+, and 180 s for CNO and He.

An increase in the energy of the electron flux was observed after the onset of dipolarization by each spacecraft (SC). After the start of dipolarization, the behaviour of energetic electron flux resembles the dynamics of the B_z field in the plasma sheet, which indicates the adiabatic acceleration of electrons, and it is consistent with the results by Malykhin et al. (2018).

Figure 1 shows the growth of the spectral index γ for electrons within 10 min after the start of dipolarization (the first front) in the energy range from 94.5 to 127.5 keV. At the moment of dipolarization, a "collapse" (sharp decrease) of the spectral index is observed in various energy ranges, the minima of which are shifted by several seconds relative to each other. For proton fluxes, the decrease in the spectral index γ during dipolarization is fixed to ~ 92 keV. At the same time, within ~ 20 min after dipolarization in the energy range of 75.3–92.2 keV, the spectral index γ fluctuates near zero.

Graphs of changes in He+ and CNO+ fluxes are similar to those for high-energy proton fluxes. We observe an increase in helium fluxes during the dipolarization of the magnetic field. As for CNO+ fluxes, the lack of a significant number of measurements for heavy ions does not allow us to draw unambiguous conclusions.

The value of the intensity of the magnetic field fluctuations at the gyrofrequencies of different types of ions was plotted in Figure 2 and

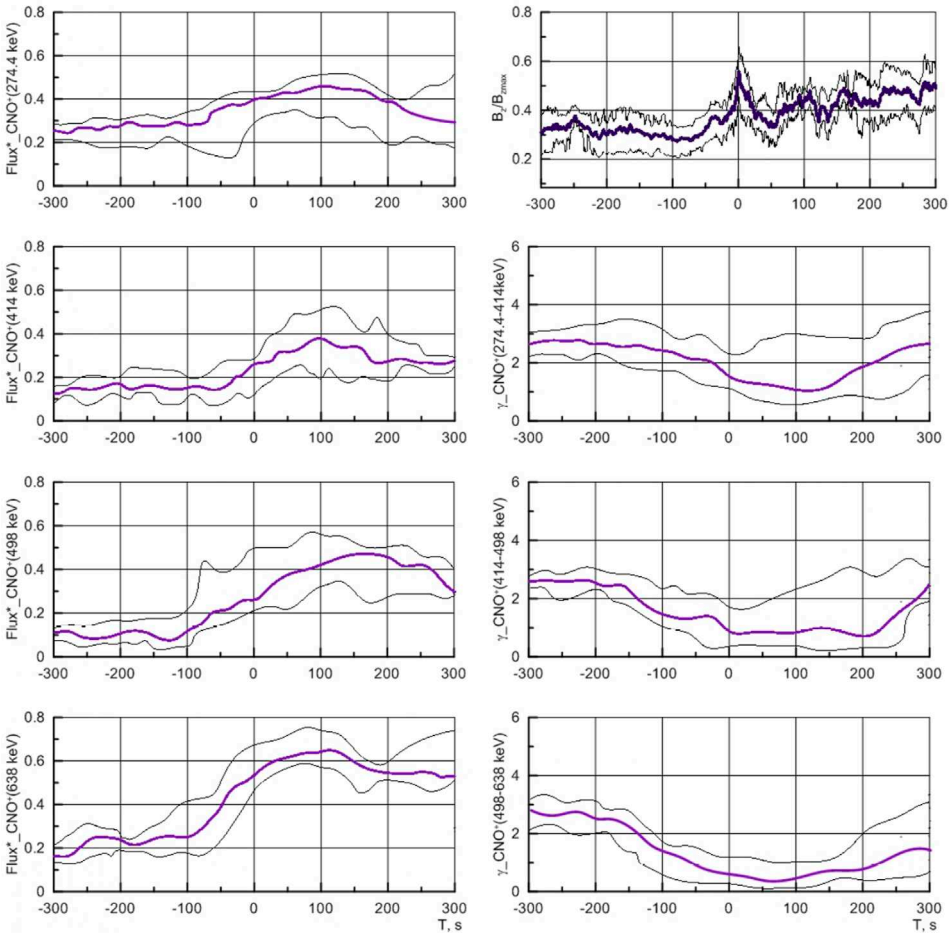

FIGURE 6
Normalized CNO fluxes (left) and spectral index (right) in different energy channels relative to the beginning of dipolarization (zero point) by the superposed epoch method. The top right panels correspond to magnetic field changes (also applied to the superimposed epoch method). Black lines show the scatter of values.

Figure 3 where we can compare the contribution of heavy ions to the processes occurring during the multiple magnetic dipolarization for the 11 September 2014 substorm.

Intensities of the magnetic field fluctuations at the gyrofrequencies of different types of ions were obtained from the slicing wavelet transform of the magnetic field over the time domain at each gyrofrequency (Figure 2). In Figure 3 we can compare the contribution of heavy ions to the processes occurring during the multiple magnetic dipolarization for the 11 September 2014 substorm.

Figure 2 obtained using continuous wavelet transform $W(t,f)$ (Morlet wavelet as mother wavelet) of magnetic field

$$W[B] = \sqrt{((W[Bx]\,W^*[Bx] + W[By]\,W^*[By] + W[Bz]\,W^*[Bz])}, \quad (2)$$

* here denotes complex conjugate, W indicates scale-normalized wavelet transform (see normalization Formula 8 in (Torrence and Compo, 1998). Bottom panel of Figure 2 $I(t)$ was built using wavelet amplitude at the frequency corresponding to gyrofrequency $g(t)$ at instant time value t: $I(t) = W(t,g(t))$. After that, we performed epoch superimposed analysis for $I(t)$ quantities for four time series (from each spacecraft) for each ion using SeaPy module functionality (Morley et al., 2014) from SpacePy python package (Figure 3). The time shift of intensity changes of different types of ions is consistent with the edge effect (Torrence and Compo, 1998).

These figures show that the highest value of the intensity of magnetic field fluctuations is observed at the gyrofrequency of oxygen ion.

3.2 Multiple events

As mentioned above, to generalize the dependence of the dynamics of different types of ions, a statistical examination was carried out by employing the superimposed epoch method. The list of available measurements for ion fluxes is shown in Supplementary Appendix Table S3.

Figure 4, Figure 5, and Figure 6 (left panel) display in different energy channels the normalized ion fluxes (for each event the flux

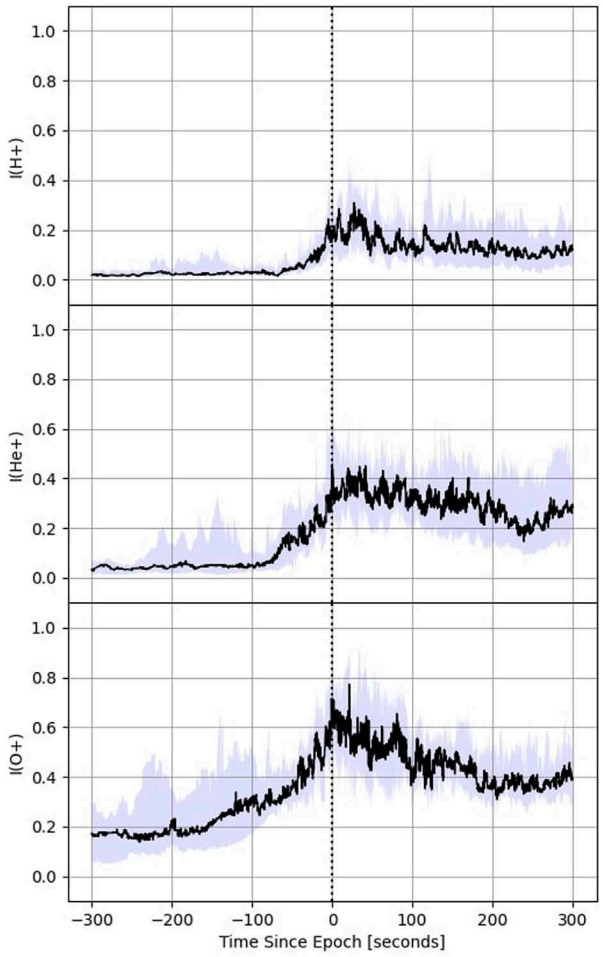

FIGURE 7
The value of the intensity of magnetic field fluctuations at different gyrofrequencies for the events of 2001–2015 (epoch method).

was normalized to the maximum value of the flux observed in a given event) obtained by the superimposed epoch method. The zero point denotes the beginning of dipolarization (the first front of dipolarization). Figure 4, Figure 5, and Figure 6 (right panel) show the value of the spectral index γ. The top right panels of Figure 4, Figure 5, Figure 6 correspond to magnetic field changes (also applied to the superimposed epoch method). The B_z magnetic field values and ion fluxes are normalized by their respective maximum values.

These figures reveal that in the case of protons, the flux shows little change to 75 keV and the spectral index was near constant for the low-energy range. A significant increase in the ions flux is observed (the maximum is shifted by ~ 1 min after the start of dipolarization) in the range of ~ 92–374 keV, while the shape of the normalized flux repeats the changes in the B_z component of the magnetic field. During this time, the spectral index, γ, calculated for this energy range decreases. A decrease in γ was observed at the same time as an increase in the flux in this range. This result indicates the energization of high-energy protons during dipolarizations. It is also worth noting that after the onset of dipolarization, the value of γ for the range 160–374 keV decreases to zero. This indicates the so-called proton spectra "flattening" in this energy range.

Changes in He+ ion fluxes in the energy range ~ 138–235 keV were very similar to changes in high-energy proton fluxes. The monotonic growth of the helium flux at ~ 138 keV, 235 keV and 315 keV begins during dipolarization. A decrease in the spectral index γ is observed up to 1 min from the zero point. That is, the acceleration of He+ lasted longer to the start of dipolarization than the acceleration of protons.

For CNO+ ions, in the considered energy channels, the largest changes are observed in the energy range of 414–638 keV. The growth of fluxes is recorded in wider time scales, as for lighter elements. A significant decrease in γ was observed in the range of energies ~ 414–638 keV. At the same time, the reduction in the spectral index γ begins before the onset of dipolarization and lasts until approximately 4 min after the beginning. In the range of energies (274—498 keV), γ has significant fluctuations after dipolarization. Since the decrease in the spectral index (γ) indicates the acceleration of the ions, it can be derived from the obtained results that the heavier ions experience stronger acceleration than the lighter ions (H+ and He+) during dipolarization.

The changes in fluxes obtained in the work are consistent with the results obtained in the work of Malykhin et al. (2019). The uniqueness of our research conducted is the comparison of changes in fluxes with changes in magnetic field intensity at gyrofrequencies of various types of ions, both for the single event and for multiple events, using the superimposed epoch method.

Figure 7 shows the values of magnetic field intensity oscillations at gyrofrequencies for various ions obtained by the superimposed epoch analysis. It is clear from these plots that the nature of the change of fluxes for protons and helium ions is very similar. An increase in wave activity precedes onset at 40 s. The increase in intensity for oxygen ion seems to be observed a few minutes before the dipolarization started. This can be explained as follows. The delta-like change in time series gives an edge effect in wavelet Morlet transform with duration $\sqrt{(}\,2)\cdot scale$ seconds. The scale is the period of gyration of the oxygen ion, with average of 100 s. So a delta-like burst, such as the first dipolarization front, will be visible in the transformation at $\sqrt{(}\,2)\cdot 100 = 144$ seconds before the onset, which is well visible in Figure 7 as a gradual increase in intensity $I(O+)$. Nevertheless, at −80…-75 s relative to the onset, there is the transition of the lower quartile of $I(O+)$ from smooth shape to more fluctuated. This means that the wavelet intensity $I(O+)$ for $t > -75$ s exceeds the wavelet edge effect. For $I(H+)$, the increase in intensity of the magnetic field begins approximately 40 s before the onset. This value exceeds the timescale of the edge effect.

4 Discussion and conclusion

In our work, we have applied a set of techniques to Cluster-II magnetic field and particle measurements to estimate the energization time dependence for protons, and heavier ions near the turbulent region of dipolarization (before the onset, and after).

The main results are:

1. After onset, wave activity remains constant for approximately 1 minute, after that gradually decreases.

2. Wave activity associated with O+ ions was observed at least 75–80 s before the dipolarization started.
3. During dipolarization CNO+ ions experience stronger acceleration than the lighter ions (H+ and He+).
4. Flux increase in the region of the dipolarization front: monotonic growth the ions flux is observed (the maximum of flux is observed at 1–1,5 min after the start of dipolarization) in the range of ~ 92–374 keV for proton; in the energy range ~ 138–235 keV for He+ and in the energy range of 414–638 keV for CNO+ ions.

Recorded flux increase before arriving dipolarization front may result from the reflection of plasma sheet ions at the dipolarization front (Zhou et al., 2011).

When analysing individual events, it was found that changes in electron fluxes inside the plasma sheet are determined by the Bz-component behaviour and indicate the adiabatic acceleration of electrons. This is consistent with results by Malykhin et al. (2018).

The increase in the fluxes of high-energy protons is consistent with the results of numerical modeling conducted by using the Rice Convection Model with an equilibrated magnetic field model for earthward BBFs in the work Yang et al. (2011). In this case, the injection boundary is well coincident with the earthward boundary of the bubble, inside which the depletion of plasma content causes the magnetic field dipolarization, and in return, the magnetic field collapse energizes particles and alters the drift paths dramatically. In turn, according to the works of Khotyaintsev et al. (2011); Grigorenko et al. (2016), Grigorenko et al. (2017) the energy transported by BBFs results in both adiabatic and non-adiabatic particle acceleration.

Superposed analysis for ion fluxes showed that changes in different energy channels differ: larger values of changes are observed for larger energy channels. Moreover, the increase in ion flows is accompanied by a spectral index decrease. This is consistent with the results obtained in the work of Malykhin et al. (2019). A decrease in γ may indicate the presence of non-adiabatic acceleration of ion population during dipolarization in 2D consideration (Pan et al., 2012). Heavy ions have efficient stochastic energization in turbulent electromagnetic fields (Zelenyi et al., 2008) and by inductive electric fields occurring in the dipolarization region. They are less affected by 3D magnetic structures and penetrate more easily into regions with vanishing magnetic fields (in the vicinity of the neutral sheet) being efficiently accelerated (Birn et al., 2012; Kronberg et al., 2014).

In (Birn et al., 2015) paper, the investigation of the ion acceleration in dipolarization events in the magnetotail, using the electromagnetic fields of an MHD simulation of magnetotail reconnection demonstrated that the ion acceleration stems from a net Lorentz force, resulting from reduced pressure gradients within a pressure pile-up region ahead of the front. Suprathermal precursor ions result from, typically multiple reflections at the front. Low-energy ions also become accelerated due to inertial drift in the direction of the small precursor electric field. An inspection of characteristic proton orbits indicated a nonadiabatic acceleration in the vicinity of the reconnection site, as well as quasi-adiabatic, betatron-like, acceleration during earthward motion in the collapsing, dipolarized field (Pan et al., 2014). For a correct description of turbulent regions of the order of proton gyroradius, it is necessary to use the self-consistent Maxwell-Vlasov equations for fields, currents, and distribution functions of charged particles.

Data availability statement

The original contributions presented in the study are included in the article/Supplementary Material, further inquiries can be directed to the corresponding author.

Author contributions

LK proposed a scientific goal for our research, conducted an interpretation of the obtained results, superimposed epoch analysis of ion flux data, and article preparation. EK made valuable suggestions about considering ion fluxes. BP made a spectral (wavelet) study and superimposed epoch analysis of magnetic field data and made visualization (SC location, wavelet, dipolarization region figure). RA and AB performed the analysis of ion flux data. IB and VF proposed useful corrections to the article text. All authors contributed to the article and approved the submitted version.

Funding

This work was supported by Grant No. 97742 of the Volkswagen Foundation (VW-Stiftung), the Royal Society International Exchanges Scheme 2021 (IES\R1\211177) and BF/30-2021. The work of EK was supported by the German Research Foundation (DFG) under number KR 4375/2-1 within SPP "Dynamic Earth".

Acknowledgments

We acknowledge Cluster Science Archive (https://www.cosmos.esa.int/ web/csa), PI and teams of FGM and RAPID instruments for providing the data.

Conflict of interest

The authors declare that the research was conducted in the absence of any commercial or financial relationships that could be construed as a potential conflict of interest.

Publisher's note

All claims expressed in this article are solely those of the authors and do not necessarily represent those of

Supplementary material

The Supplementary Material for this article can be found online at: https://www.frontiersin.org/articles/10.3389/fspas.2023.1226200/full#supplementary-material

References

Alexandrova, O., Chen, C. H. K., Sorriso-Valvo, L., Horbury, T. S., and Bale, S. D. (2013). Solar wind turbulence and the role of ion instabilities. *Space Sci. Rev.* 178, 101–139. doi:10.1007/s11214-013-0004-8

Angelopoulos, V., Baumjohann, W., Kennel, C., Coroniti, F. V., Kivelson, M., Pellat, R., et al. (1992). Bursty bulk flows in the inner central plasma sheet. *J. Geophys. Res. Space Phys.* 97, 4027–4039. doi:10.1029/91ja02701

Arzoumanian, D., André, P., Didelon, P., Könyves, V., Schneider, N., Men'shchikov, A., et al. (2011). Characterizing interstellar filaments with herschel in ic 5146. *Astronomy Astrophysics* 529, L6. doi:10.1051/0004-6361/201116596

Balogh, A., Carr, C. M., Acuna, M., Dunlop, M., Beek, T., Brown, P., et al. (2001). The cluster magnetic field investigation: overview of in-flight performance and initial results. *Ann. Geophys. Copernic. GmbH)* 19, 1207–1217. doi:10.5194/angeo-19-1207-2001

Birn, J., Artemyev, A., Baker, D., Echim, M., Hoshino, M., and Zelenyi, L. (2012). Particle acceleration in the magnetotail and aurora. *Space Sci. Rev.* 173, 49–102. doi:10.1007/s11214-012-9874-4

Birn, J., Runov, A., and Hesse, M. (2015). Energetic ions in dipolarization events. *J. Geophys. Res. Space Phys.* 120, 7698–7717. doi:10.1002/2015ja021372

Borovsky, J. E., Nemzek, R. J., and Belian, R. D. (1993). The occurrence rate of magnetospheric-substorm onsets: random and periodic substorms. *J. Geophys. Res. Space Phys.* 98, 3807–3813. doi:10.1029/92ja02556

Brandenburg, A., and Nordlund, Å. (2011). Astrophysical turbulence modeling. *Rep. Prog. Phys.* 74, 046901. doi:10.1088/0034-4885/74/4/046901

Bruno, R., Carbone, V., Oliveira, P. L., and Lourenço-de-Oliveira, R. (2013). Foreword. *Living Rev. Sol. Phys.* 10, 1–208. doi:10.1590/0074-0276130585

Camporeale, E., and Burgess, D. (2011). The dissipation of solar wind turbulent fluctuations at electron scales. *Astrophysical J.* 730, 114. doi:10.1088/0004-637x/730/2/114

Chandran, B. D., Li, B., Rogers, B. N., Quataert, E., and Germaschewski, K. (2010). Perpendicular ion heating by low-frequency alfvén-wave turbulence in the solar wind. *Astrophysical J.* 720, 503–515. doi:10.1088/0004-637x/720/1/503

Chandran, B., Verscharen, D., Quataert, E., Kasper, J., Isenberg, P., and Bourouaine, S. (2013). Stochastic heating, differential flow, and the alpha-to-proton temperature ratio in the solar wind. *Astrophysical J.* 776, 45. doi:10.1088/0004-637x/776/1/45

Chasapis, A., Retinò, A., Sahraoui, F., Vaivads, A., Khotyaintsev, Y. V., Sundkvist, D., et al. (2015). Thin current sheets and associated electron heating in turbulent space plasma. *Astrophysical J. Lett.* 804, L1. doi:10.1088/2041-8205/804/1/l1

Delzanno, G. L., Borovsky, J. E., Henderson, M. G., Resendiz Lira, P. A., Roytershteyn, V., and Welling, D. T. (2021). The impact of cold electrons and cold ions in magnetospheric physics. *J. Atmos. Solar-Terrestrial Phys.* 220, 105599. doi:10.1016/j.jastp.2021.105599

Grigorenko, E., Kronberg, E., Daly, P., Ganushkina, N. Y., Lavraud, B., Sauvaud, J. A., et al. (2016). Origin of low proton-to-electron temperature ratio in the earth's plasma sheet. *J. Geophys. Res. Space Phys.* 121, 9985–10010. doi:10.1002/2016ja022874

Grigorenko, E., Kronberg, E., and Daly, P. (2017). Heating and acceleration of charged particles during magnetic dipolarizations. *Cosmic Res.* 55, 57–66. doi:10.1134/s0010952517010063

Grigorenko, E., Malykhin, A. Y., Kronberg, E., Malova, K. V., and Daly, P. (2015). Acceleration of ions to suprathermal energies by turbulence in the plasmoid-like magnetic structures. *J. Geophys. Res. Space Phys.* 120, 6541–6558. doi:10.1002/2015ja021314

Hajivassiliou, C. A. (1992). Distribution of plasma turbulence in our galaxy derived from radio scintillation maps. *Nature* 355, 232–234. doi:10.1038/355232a0

Imada, S., Nakamura, R., Daly, P., Hoshino, M., Baumjohann, W., Mühlbachler, S., et al. (2007). Energetic electron acceleration in the downstream reconnection outflow region. *J. Geophys. Res. Space Phys.* 112, 11847. doi:10.1029/2006ja011847

Ipavich, F., Galvin, A., Gloeckler, G., Hovestadt, D., Klecker, B., and Scholer, M. (1984). Energetic (>100 kev) o+ ions in the plasma sheet. *Geophys. Res. Lett.* 11, 504–507. doi:10.1029/gl011i005p00504

Karimabadi, H., Roytershteyn, V., Wan, M., Matthaeus, W., Daughton, W., Wu, P., et al. (2013). Coherent structures, intermittent turbulence, and dissipation in high-temperature plasmas. *Phys. Plasmas* 20, 012303. doi:10.1063/1.4773205

Kasper, J., Lazarus, A., and Gary, S. (2008). Hot solar-wind helium: direct evidence for local heating by alfvén-cyclotron dissipation. *Phys. Rev. Lett.* 101, 261103. doi:10.1103/physrevlett.101.261103

Keika, K., Brandt, P., Nosé, M., and Mitchell, D. (2011). Evolution of ring current ion energy spectra during the storm recovery phase: implication for dominant ion loss processes. *J. Geophys. Res. Space Phys.* 116, 15628. doi:10.1029/2010ja015628

Khotyaintsev, Y. V., Cully, C., Vaivads, A., André, M., and Owen, C. (2011). Plasma jet braking: energy dissipation and nonadiabatic electrons. *Phys. Rev. Lett.* 106, 165001. doi:10.1103/physrevlett.106.165001

Kistler, L., Möbius, E., Klecker, B., Gloeckler, G., Ipavich, F., and Hamilton, D. (1990). Spatial variations in the suprathermal ion distributions during substorms in the plasma sheet. *J. Geophys. Res. Space Phys.* 95, 18871–18885. doi:10.1029/ja095ia11p18871

Kozak, L., Petrenko, B., Kronberg, E. A., Grigorenko, E., Kozak, P., and Reka, K. (2020). Variations in the plasma parameters of the earth's magnetotail during substorm initiation. *Kinemat. Phys. Celest. Bodies* 36, 94–102. doi:10.3103/s0884591320020051

Kozak, L., Petrenko, B., Kronberg, E., Grigorenko, E., and Lui, A. (2018a). Characteristics of the turbulence processes in the magnetohydrodynamic environment. *Athens J. Sci.* 5, 101–124. doi:10.30958/ajs.5-2-1

Kozak, L., Petrenko, B., Kronberg, E., Grigorenko, E., Lui, E., and Cheremnykh, S. (2018b). Spectra of turbulence during the dipolarization of the magnetic field. *Kinemat. Phys. Celest. Bodies* 34, 258–269. doi:10.3103/s0884591318050021

Kozak, L., Petrenko, B., Lui, A., Kronberg, E. A., and Daly, P. W. (2021). Processes in the current disruption region: from turbulence to dispersion relation. *J. Geophys. Res. Space Phys.* 126, e2020JA028404. doi:10.1029/2020ja028404

Kozak, L. V., Petrenko, B. A., Lui, A. T., Kronberg, E. A., Grigorenko, E. E., and Prokhorenkov, A. S. (2018c). Turbulent processes in the earth's magnetotail: spectral and statistical research. *Ann. Geophys. Copernic. GmbH)* 36, 1303–1318. doi:10.5194/angeo-36-1303-2018

Kronberg, E. A., Ashour-Abdalla, M., Dandouras, I., Delcourt, D. C., Grigorenko, E. E., Kistler, L. M., et al. (2014). Circulation of heavy ions and their dynamical effects in the magnetosphere: recent observations and models. *Space Sci. Rev.* 184, 173–235. doi:10.1007/s11214-014-0104-0

Kronberg, E. A., and Daly, P. W. (2013). Spectral analysis for wide energy channels. *Geoscientific Instrum. Methods Data Syst.* 2, 257–261. doi:10.5194/gi-2-257-2013

Kronberg, E. A., Kis, A., Klecker, B., Daly, P. W., and Lucek, E. A. (2009). Multipoint observations of ions in the 30–160 kev energy range upstream of the earth's bow shock. *J. Geophys. Res. Space Phys.* 114, 13754. doi:10.1029/2008ja013754

Kronberg, E., Grigorenko, E., Turner, D., Daly, P., Khotyaintsev, Y., and Kozak, L. (2017). Comparing and contrasting dispersionless injections at geosynchronous orbit during a substorm event. *J. Geophys. Res. Space Phys.* 122, 3055–3072. doi:10.1002/2016ja023551

Malykhin, A. Y., Grigorenko, E. E., Kronberg, E. A., Daly, P. W., and Kozak, L. V. (2019). Acceleration of protons and heavy ions to suprathermal energies during dipolarizations in the near-earth magnetotail. *Ann. Geophys. Copernic. GmbH)* 37, 549–559. doi:10.5194/angeo-37-549-2019

Malykhin, A. Y., Grigorenko, E. E., Kronberg, E. A., Koleva, R., Ganushkina, N. Y., Kozak, L., et al. (2018). Contrasting dynamics of electrons and protons in the near-earth plasma sheet during dipolarization. *Ann. Geophys. Copernic. GmbH)* 36, 741–760. doi:10.5194/angeo-36-741-2018

Maneva, Y., Viñas, A., and Ofman, L. (2013). Turbulent heating and acceleration of he++ ions by spectra of alfvén-cyclotron waves in the expanding solar wind: 1.5-d hybrid simulations. *J. Geophys. Res. Space Phys.* 118, 2842–2853. doi:10.1002/jgra.50363

Mitchell, D. G., Brandt, P. C., Roelof, E. C., Hamilton, D. C., Retterer, K. C., Mende, S., et al. (2003). Global imaging of o+ from image/hena. *Magnetos. Imaging—The Image Prime Mission.* 109, 63–75. doi:10.1023/b:spac.0000007513.55076.00

Möbius, E., Scholer, M., Klecker, B., Hovestadt, D., and Gloeckler, G. (1987). Acceleration of ions of ionospheric origin in the plasma sheet during substorm activity. *Magnetotail Phys.* 1, 231–234.

Morley, S., Koller, J., Welling, D., Larsen, B., and Niehof, J. (2014). *Spacepy: python-based tools for the space science community*. Michgan, ASCL: Astrophysics Source Code Library. https://ascl.net/1401.002

Nakamura, R., Baumjohann, W., Klecker, B., Bogdanova, Y., Balogh, A., Rème, H., et al. (2002). Motion of the dipolarization front during a flow burst event observed by cluster. *Geophys. Res. Lett.* 29, 3-1–3-4. doi:10.1029/2002gl015763

Pan, Q., Ashour-Abdalla, M., El-Alaoui, M., Walker, R. J., and Goldstein, M. L. (2012). Adiabatic acceleration of suprathermal electrons associated with dipolarization fronts. *J. Geophys. Res. Space Phys.* 117, 18156. doi:10.1029/2012ja018156

Pan, Q., Ashour-Abdalla, M., Walker, R. J., and El-Alaoui, M. (2014). Ion energization and transport associated with magnetic dipolarizations. *Geophys. Res. Lett.* 41, 5717–5726. doi:10.1002/2014gl061209

Retinò, A., Sundkvist, D., Vaivads, A., Mozer, F., André, M., and Owen, C. (2007). *In situ* evidence of magnetic reconnection in turbulent plasma. *Nat. Phys.* 3, 235–238. doi:10.1038/nphys574

Runov, A., Angelopoulos, V., Sitnov, M., Sergeev, V., Bonnell, J., McFadden, J., et al. (2009). Themis observations of an earthward-propagating dipolarization front. *Geophys. Res. Lett.* 36, L14106. doi:10.1029/2009gl038980

Runov, A., Angelopoulos, V., Sitnov, M., Sergeev, V., Nakamura, R., Nishimura, Y., et al. (2011). Dipolarization fronts in the magnetotail plasma sheet. *Planet. Space Sci.* 59, 517–525. doi:10.1016/j.pss.2010.06.006

Saur, J. (2004). Turbulent heating of jupiter's middle magnetosphere. *Astrophysical J.* 602, L137–L140. doi:10.1086/382588

Sergeev, V., Angelopoulos, V., and Nakamura, R. (2012). Recent advances in understanding substorm dynamics. *Geophys. Res. Lett.* 39, 859. doi:10.1029/2012gl050859

Servidio, S., Matthaeus, W., Shay, M., Cassak, P., and Dmitruk, P. (2009). Magnetic reconnection in two-dimensional magnetohydrodynamic turbulence. *Phys. Rev. Lett.* 102, 115003. doi:10.1103/physrevlett.102.115003

Servidio, S., Valentini, F., Califano, F., and Veltri, P. (2012). Local kinetic effects in two-dimensional plasma turbulence. *Phys. Rev. Lett.* 108, 045001. doi:10.1103/physrevlett.108.045001

Shiokawa, K., Baumjohann, W., and Haerendel, G. (1997). Braking of high-speed flows in the near-earth tail. *Geophys. Res. Lett.* 24, 1179–1182. doi:10.1029/97gl01062

Telloni, D., Antonucci, E., and Dodero, M. A. (2007). Oxygen temperature anisotropy and solar wind heating above coronal holes out to 5*R*☉. *Astronomy Astrophysics* 476, 1341–1346. doi:10.1051/0004-6361:20077660

TenBarge, J. M., and Howes, G. (2013). Current sheets and collisionless damping in kinetic plasma turbulence. *Astrophysical J. Lett.* 771, L27. doi:10.1088/2041-8205/771/2/l27

Torrence, C., and Compo, G. P. (1998). A practical guide to wavelet analysis. *Bull. Am. Meteorological Soc.* 79, 61–78. doi:10.1175/1520-0477(1998)079<0061:apgtwa>2.0.co;2

Uritsky, V., Slavin, J., Khazanov, G., Donovan, E., Boardsen, S., Anderson, B., et al. (2011). Kinetic-scale magnetic turbulence and finite larmor radius effects at mercury. *J. Geophys. Res. Space Phys.* 116, 16744. doi:10.1029/2011ja016744

Von Papen, M., Saur, J., and Alexandrova, O. (2014). Turbulent magnetic field fluctuations in saturn's magnetosphere. *J. Geophys. Res. Space Phys.* 119, 2797–2818. doi:10.1002/2013ja019542

Wilken, B., Daly, P., Mall, U., Aarsnes, K., Baker, D., Belian, R., et al. (2001). First results from the rapid imaging energetic particle spectrometer on board cluster. *Ann. Geophys. Copernic. GmbH)* 19, 1355–1366. doi:10.5194/angeo-19-1355-2001

Yang, J., Toffoletto, F., Wolf, R., and Sazykin, S. (2011). Rcm-e simulation of ion acceleration during an idealized plasma sheet bubble injection. *J. Geophys. Res. Space Phys.* 116, 16346. doi:10.1029/2010ja016346

Zaharia, S., Cheng, C., and Johnson, J. R. (2000). Particle transport and energization associated with substorms. *J. Geophys. Res. Space Phys.* 105, 18741–18752. doi:10.1029/1999ja000407

Zelenyi, L., Artemyev, A., Malova, H., Milovanov, A. V., and Zimbardo, G. (2008). Particle transport and acceleration in a time-varying electromagnetic field with a multi-scale structure. *Phys. Lett. A* 372, 6284–6287. doi:10.1016/j.physleta.2008.08.035

Zhou, X. Z., Angelopoulos, V., Sergeev, V., and Runov, A. (2011). On the nature of precursor flows upstream of advancing dipolarization fronts. *J. Geophys. Res. Space Phys.* 116, 16165. doi:10.1029/2010ja016165